A Hybrid Algorithm for the Baer-Nunziato Model Using the Riemann Invariants *

Smadar Karni † Gerardo Hernández-Dueñas †

Abstract

The paper considers the Baer-Nunziato model for two-phase flow in porous media, with discontinuous porosity. Computing solutions of the Riemann problem rests on capturing the jump in the solution across the porosity jump. A recent study [8] showed that numerical discretizations may fail to correctly capture the jump conditions across the so-called compaction wave, and yield incorrect solutions. We have formulated the Baer-Nunziato system using the Riemann invariants across the porosity jump, and propose a hybrid algorithm that uses the Riemann invariants formulation across the compaction wave, and the conservative formulation away from the compaction wave. The paper motivates and describes the hybrid scheme and present numerical results.

1 Introduction

The generic formation of shock waves in solutions of nonlinear hyperbolic conservation laws necessitates the reliance on conservative formulation in numerical computations. Isolated waves are characterized by flow invariances which simplify the structure of the underlying flow but are not readily seen by the conservative formulations. Multimaterial flows are one such example. Naive discretizations based on conservative flow formulations fail to respect the fact that the pressure and velocity are constant across the material front, and are often plagued by pressure and other oscillations across propagating material interfaces. Recognizing and respecting material front data is easily accomplished by writing the evolution equations directly in terms of the pressure and velocity variables, a property which is trivially inherited by *any* consistent discretization of the pressure (and velocity) evolution equation ([1, 2, 3]). The pressure and the velocity are the Riemann invariants across material fronts, and formulating the flow equations in terms of these variables brings out the underlying simple structure of the flow, as these variables simply 'do nothing' across the front and in doing nothing, provide the correct statement of the jump conditions. Another example is near steady-state computations of shallow water flows. Here, the mass flow rate and total energy are constant in the smooth steady-state limit. It has been recognized that incorporating these variables into the design of the numerical scheme makes it possible for numerical scheme to recognize and respect certain steady-state flows, which result in better accuracy for near steady-state flows ([9, 12]).

In this paper, we consider the Baer-Nunziato model for two-phase flow in porous media, with piecewise constant porosity. A schematic is given in Figure 1. Solutions for the Riemann problem consist of two single-phase compressible Euler sub-systems and an additional wave called a compaction wave, which carries changes in porosity and provides the means through which the two phases are coupled. Computing solutions of the Riemann problem rests on capturing the jump conditions across the porosity jump. A recent numerical study [8], showed that numerical methods may have difficulties to compute it correctly, and suggested that this failure is due to the inability of the conservative formulation to preserve constant gas entropy across the compaction wave front, resulting in incorrect jump across the wave front and yielding incorrect solution.

*Work supported in part by NSF DMS #0609766 and by CONACYT #160147

†Department of Mathematics, University of Michigan, Ann Arbor, MI 48109-1043.

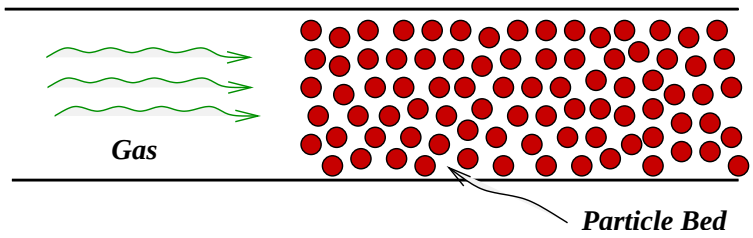

Figure 1: Gas flow over a porous particle bed.

The gas entropy η is one of the Riemann invariants across the porosity jump. The evolution equation for the gas entropy is given by

$$\frac{\partial \eta}{\partial t} + u\frac{\partial \eta}{\partial x} = 0,$$

and has the attractive property that if the gas entropy is constant in the data, $\eta_x = 0$, it will remain constant in the solution $\eta_t = 0$, a property which is inherited by *any* numerical discretization. Although not in conservation form, this equation is *exact* across a compaction wave front, and provides a way of imposing the jump conditions across it. We follow the rationale of the above examples and formulate the Baer-Nunziato model in terms of the Riemann invariants across the compaction wave. We examine the merit of a hybrid algorithm that uses the Riemann invariants formulation across the compaction wave, and the conservative formulation away from the compaction wave.

The paper is organized as follows: In Section §2, we describe the Baer-Nunziato flow model, as well as a related reduced flow model that is obtained under simplifying assumptions. Section §3 discusses the numerical scheme, Section §4 focuses on the reduced model, motivates the use of the Riemann invariants (RI) in the numerical scheme and proposes a conservative/RI hybrid strategy. Section §5 generalizes this hybrid approach to the Baer-Nunziato model and presents numerical results.

2 The Equations

2.1 The Baer-Nunziato Model

The Baer-Nunziato (BN) model was originally proposed in [6] to describe the deflagration-to-detonation transition in reactive granular material. Neglecting the terms due to combustion processes, drag and heat transfer, and focusing on the hydrodynamic part of the system, the system is given by

$$\begin{aligned}
&(\phi_g\rho_g)_t + (\phi_g\rho_g u_g)_x = 0\\
&(\phi_g\rho_g u_g)_t + (\phi_g\rho_g u_g^2 + \phi_g p_g)_x = p_g(\phi_g)_x\\
&(\phi_g E_g)_t + (u_g(\phi_g E_g + \phi_g p_g))_x = p_g u_s(\phi_g)_x\\
&(\phi_s\rho_s)_t + (\phi_s\rho_s u_s)_x = 0\\
&(\phi_s\rho_s u_s)_t + (\phi_s\rho_s u_s^2 + \phi_s p_s)_x = p_g(\phi_s)_x\\
&(\phi_s E_s)_t + (u_s(\phi_s E_s + \phi_s p_s))_x = p_g u_s(\phi_s)_x\\
&(\phi_s)_t + u_s(\phi_s)_x = 0
\end{aligned} \tag{1}$$

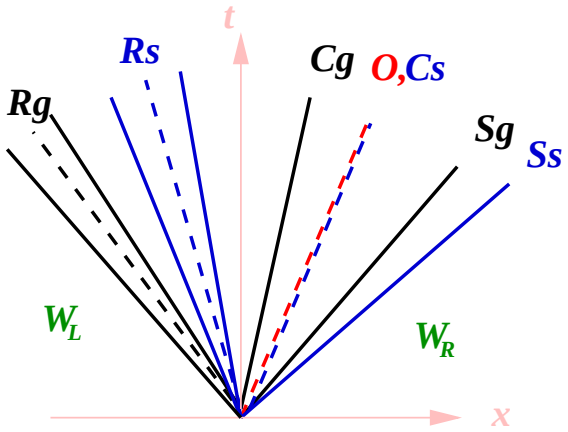

Figure 2: Typical solution for the Riemann problem for the BN system (1) .

Here the subscript $(\ )_{g,s}$ denote gas and solid phases respectively, $\rho,\ u,\ p$ and E denote the density, velocity, pressure and energy of the respective phases, both assumed ideal fluids and satisfy the Equation of State

$$E = \frac{1}{2}\rho u^2 + \frac{p}{\gamma - 1}, \tag{2}$$

where γ is the ratio of specific heats, and ϕ is the porosity, satisfying

$$\phi_g + \phi_s = 1\ . \tag{3}$$

The coupling between the phases occurs through changes in porosity. The system is inherently non-conservative due to momentum and energy exchange between the phases. The underlying conservation is revealed upon addition of the momenta (energy) equations of the individual phases. The presence of the non-conservative terms has major consequences both theoretically and computationally.

The eigenvalues and eigenvectors for this system are given by

$$\Lambda = diag\left(u_g - c_g, u_g, u_g + c_g, u_s - c_s, u_s, u_s + c_s, u_s\right), \tag{4}$$

$$R^C = \begin{pmatrix} 1 & 1 & 1 & 0 & 0 & 0 & \rho_g c_g^2 \\ u_g - c_g & u_g & u_g + c_g & 0 & 0 & 0 & \rho_g c_g^2 u_s \\ h_g - u_g c_g & \frac{1}{2}u_g^2 & h_g + u_g c_g & 0 & 0 & 0 & \rho_g v_g^2 h_g - \rho_g u_g c_g^2 v_g - (v_g^2 - c_g^2)E_g \\ 0 & 0 & 0 & 1 & 1 & 1 & (v_g^2 - c_g^2)\left(\rho_s + \frac{p_g - p_s}{c_s^2}\right) \\ 0 & 0 & 0 & u_s - c_s & u_s & u_s + c_s & (v_g^2 - c_g^2)\left(\rho_s + \frac{p_g - p_s}{c_s^2}\right) u_s \\ 0 & 0 & 0 & h_s - u_s c_s & \frac{1}{2}u_s^2 & h_s + u_s c_s & (v_g^2 - c_g^2)\left(E_s + \frac{p_g - p_s}{c_s^2} h_s\right) \\ 0 & 0 & 0 & 0 & 0 & 0 & v_g^2 - c_g^2 \end{pmatrix}, \tag{5}$$

here $v_g = u_g - u_s$, $h = \frac{1}{2}u^2 + \frac{c^2}{\gamma - 1}$ is the specific enthalpy and $c = \sqrt{\frac{\gamma p}{\rho}}$ the speed of sound. We observe the three familiar waves in each phase, and an additional so-called compaction wave. A solution for a typical

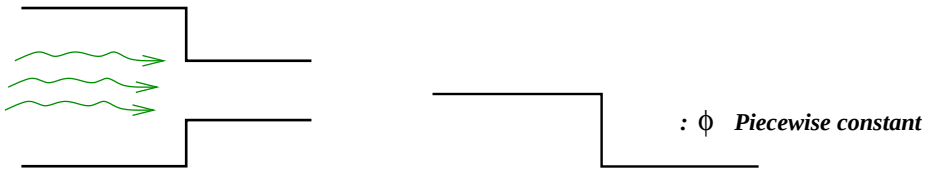

Figure 3: Gas flow through a channel with discontinuous area variation.

Riemann problem is illustrated in Figure 2, where we have used $(\cdot)_{g,s}$ to denote the gas and solid phases respectively, and O to denote the compaction wave. We note that in this model, porosity changes are carried with the solid phase, resulting in u_s being a double eigenvalue, corresponding to a solid contact discontinuity *and* a compaction wave. The Riemann invariants across a compaction wave are [6, 7, 5, 8]

$$[u_s] = 0\ , [\eta_g] = 0\ ,\quad [\eta_s] = 0\ ,\quad [Q] = 0\ ,\quad [P] = 0\ ,\quad [H] = 0\ ,$$

here $\eta = \frac{p}{\rho^\gamma}$ is the entropy, $Q = \phi_g \rho_g v_g$ is the gas mass flux, $H = \frac{1}{2}v_g^2 + \frac{c_g^2}{\gamma_g - 1}$ is the gas enthalpy and $P = \phi_g p_g + \phi_s p_s + \phi_g \rho_g v_g^2$ is the sum of phase momenta fluxes as observed *in the frame of reference of the compaction wave* moving with speed u_s.

We note that the compaction wave is a linearly degenerate field, $\lambda = u_s$ is constant across the wave, and the solution simply traslates with the constant speed u_s. In this case, the Hugoniot curve and the integral curve agree, and the Riemann invariants also represent conserved quantities across a porosity jump. See [7, 11] for more details.

The system is only conditionally hyperbolic, and may lose hyperbolicity if $v_g^2 = c_g^2$. This corresponds, for example, to a flow in which the gas rarefaction straddles the compaction wave. In this case, the set of eigenvectors is no longer linearly independent. For certain data, the solution for the Riemann problem may be nonunique, and continuous dependence on coefficients may be used to select the physically relevant solution (for further discussion, see [6, 7, 5, 8, 14]).

2.2 Reduced Flow Model

If the solid phase is assumed stationary, $u_s = 0$, and incompressible, $\delta\rho_s = 0$, the porosity ϕ becomes a function of x alone and system (1) reduces to

$$\begin{aligned} (\phi\rho)_t &+ (\phi\rho u)_x = 0 \\ (\phi\rho u)_t &+ (\phi\rho u^2 + \phi p)_x = p\phi_x \\ (\phi E)_t &+ (u(\phi E + \phi p))_x = 0, \end{aligned} \tag{6}$$

where we have removed the subscripts $()_g$ to avoid notation clutter. Note that the role of $\phi = \phi(x)$ here is that of a variable coefficient. The reduced system (6) is in fact the Euler equations through a channel with variable geometry. Here the porosity can be viewed as a variable cross sectional area. We consider gas flow through porous media with piece-wise constant porosity $\phi(x)$, as illustrated as in Figure 3. This model is studied in [4], and was considered as a simplification of the BN system (1) in [8].

System (6) can be rewritten in quasilinear form using the primitive variables

$$W_t^P + A(W^P)W_x^P = 0,$$

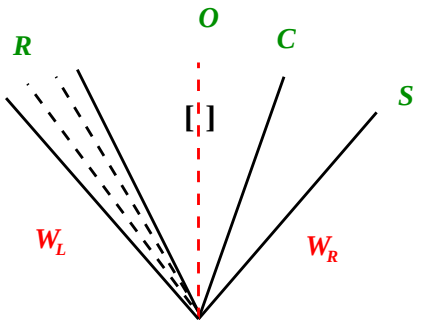

Figure 4: Schematic of the Riemann problem of the reduced system (6).

where

$$W^P = \begin{pmatrix} \rho \\ u \\ p \\ \phi \end{pmatrix}, \quad A(W^P) = \begin{pmatrix} u & \rho & 0 & \frac{\rho u}{\phi} \\ 0 & u & \frac{1}{\rho} & 0 \\ 0 & \gamma p & u & \frac{\gamma p u}{\phi} \\ 0 & 0 & 0 & 0 \end{pmatrix}. \tag{7}$$

The eigenvectors and eigenvalues of the system are

$$R^P = \begin{pmatrix} 1 & 1 & 1 & -\rho u^2 \\ -c/\rho & 0 & c/\rho & uc^2 \\ c^2 & 0 & c^2 & -\rho u^2 c^2 \\ 0 & 0 & 0 & \phi(u^2 - c^2) \end{pmatrix} \qquad \Lambda = \text{diag}\left(u - c,\ u,\ u + c,\ 0\right). \tag{8}$$

The first three eigenfields are analogous to single-phase Euler flow. The last eigenvector corresponds to the stationary porosity interface, across which the jump conditions are [6, 7, 4, 8]

$$[\phi \rho u] = 0, \quad [\eta] = 0, \quad [h] = 0. \tag{9}$$

We note that while the compaction wave is linearly degenerate, it does not behave like a contact discontinuity. More specifically, it can be seen from (9) that if $[p] = 0$ as is the case across a contact discuntinuity, then (9b) implies $[\rho] = 0$, (9c) then implies $[u] = 0$ and (9a) then implies that $[\phi] = 0$. It follows that if $[\phi] \neq 0$, as is the case across the porosity jump, $p,\ \rho$ and u are generally discontinuous (see discussion in [8]).

Figure 4 shows a typical solution of a Riemann problem for the system (6) consisting of a rarefaction (R), a shock (S), a contact wave (C) and a compaction wave (O). Exact solutions to Riemann data may be obtained by embedding the interface jump conditions (9) in a rootfinding iteration of two single-phase Riemann solutions. Alternatively, one can start from a given state, say W_R, and build up a solution of a pre-determined wave structure using known relationships that hold across the single-phase wavefronts and porosity jump. We note that for certain data, the solution for the Riemann problem is not unique, and some consideration of continuous dependence on coefficients may be used to select the relevant solution (see [4] for more details). In the numerical examples in this paper, we have used both approaches to generate exact solutions. When using an iterative solver for given left/right states, we have used the rootfinding algorithm proposed in [14].

3 Numerical Scheme

The hybrid algorithm that we propose is formulated at the differential equations level, and may be discretized by one's favorite choice of scheme. The conservative formulation (1) has the form

$$W_t + F(W)_x = S,$$

where $F(W)$ is the flux function and S denotes the nonconservative products. The examples in the next two sections were obtained using a wave propagation Roe-type upwind scheme [13]

$$W_j^{n+1} = W_j^n - \frac{\Delta t}{\Delta x}\left\{A^+_{j-\frac{1}{2}}\left(W_j^n - W_{j-1}^n\right) + A^-_{j+\frac{1}{2}}\left(W_{j+1}^n - W_j^n\right)\right\} \tag{10}$$

with

$$A^+\Delta W = \sum_k \alpha_k \lambda_k^+ r_k \ , \qquad \lambda_k^+ = \max\left(0,\ \lambda_k\right)$$

$$A^-\Delta W = \sum_k \alpha_k \lambda_k^- r_k \ , \qquad \lambda_k^- = \min\left(0,\ \lambda_k\right)$$

where r_k and λ_k are the eigenvectors and eigenvalues of the Jacobian matrix $A = F^{'}(W)$, and α_k are the wave strengths determined by $\Delta W = \sum_k \alpha_k r_k$.

The Roe linearization is used where applicable, other variables are linearized by simple arithmetic averages

$$\bar{\rho} = \sqrt{\rho_L \rho_R}$$

$$\bar{u} = \frac{\sqrt{\rho_L}u_L + \sqrt{\rho_R}u_R}{\sqrt{\rho_L} + \sqrt{\rho_R}} \qquad \bar{h} = \frac{\sqrt{\rho_L}h_L + \sqrt{\rho_R}h_R}{\sqrt{\rho_L} + \sqrt{\rho_R}}$$

$$\overline{c^2} = (\gamma - 1)\left(\bar{h} - \frac{1}{2}\bar{u}^2\right) \qquad \bar{\eta} = \frac{\eta_L + \eta_R}{2}$$

The conservative formulation of the model is solved in a split-step algorithm, the upwind scheme (10) is applied to the Jacobian matrix $A = F'(W^C)$, the source terms in the momentum and energy equations are approximated by

$$\begin{aligned} p\,\frac{\partial \phi}{\partial x} &\approx \frac{1}{2}\left(p_{j-\frac{1}{2}}\frac{\phi_{j+1}-\phi_{j-1}}{\Delta x} + p_{j+\frac{1}{2}}\frac{\phi_{j+1}-\phi_j}{\Delta x}\right) \\ up\,\frac{\partial \phi}{\partial x} &\approx \frac{1}{2}\left(u_{j-\frac{1}{2}}p_{j-\frac{1}{2}}\frac{\phi_j-\phi_{j-1}}{\Delta x} + u_{j+\frac{1}{2}}p_{j+\frac{1}{2}}\frac{\phi_{j+1}-\phi_j}{\Delta x}\right), \end{aligned} \tag{11}$$

where $(\cdot)_{j\pm\frac{1}{2}} = \frac{1}{2}\left\{(\cdot)_j + (\cdot)_{j\pm1}\right\}$. The compaction wave equation in (1) is approximated by the upwind scheme. The nonconservative formulations based on the Riemann invariants are approximated by (10), with the matrix A denoting the coefficient matrix in the quasilinear form of the equations.

4 Numerics - Reduced System

In the following numerical examples, the initial data is given in terms of $W = (\rho,\ u,\ p,\ \phi)$. Consider the Riemann problem

$$\begin{aligned} W_L &= (1.6934 \times 10^2,\ 0,\ 2.96 \times 10^8,\ 0.25) \\ W_R &= (7.6278 \times 10^{-1},\ 0,\ 1.00 \times 10^5,\ 1.00) \end{aligned} \tag{12}$$

corresponding to a rarefaction wave that straddles the porosity interface, followed by a right moving contact discontinuity and a shock. This problem was considered in [8], here $\gamma = 1.23$, $CFL = 0.8$ and the grid has 2000 points. The numerical solution based on the conservative formulation and the exact solution are shown in Figure 5 (left). The computation is in noticeable error, the solution appears to jump incorrectly across the porosity change yielding an incorrect solution. As can be seen in the figure and was put forward in [8] by way of explanation, the gas entropy fails to remain constant across the porosity jump, resulting in incorrect jump across the wave front and yielding incorrect solution. In the next section, we propose a more direct way to impose the jump conditions across the porosity jump by formulating the equations in terms of the entropy.

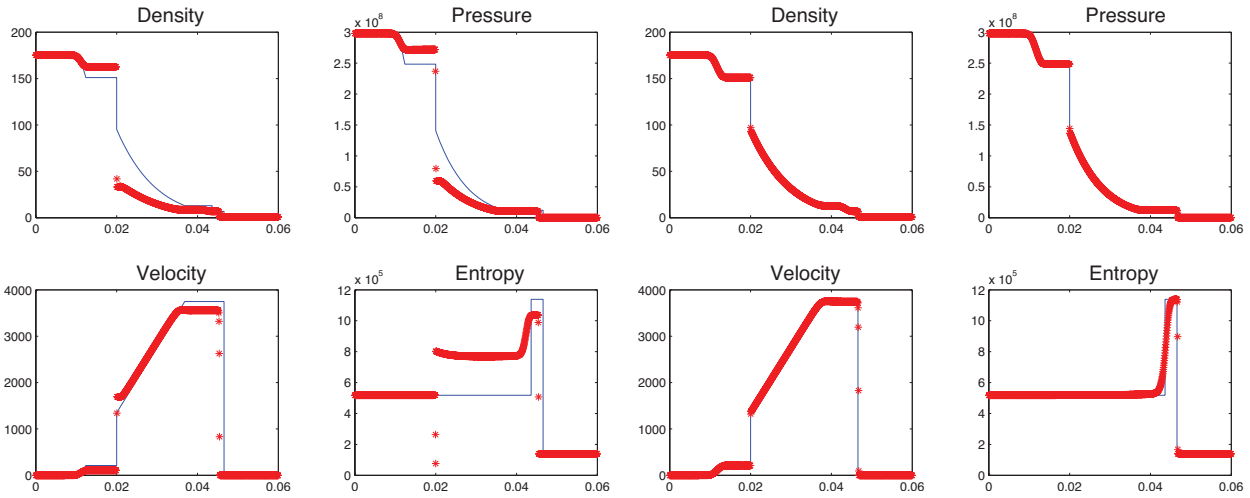

Figure 5: Computed and exact solution for initial data (12) by the conservative (left) and hybrid (right) formulations.

4.1 A Hybrid Formulation

By differentiating $\eta = p/\rho^\gamma$ and using the primitive variable formulation (7) it is straightforward to derive the entropy evolution equation

$$\eta_t + u\eta_x = 0. \tag{13}$$

Equation (13) has the attractive property that when applied to data in which η is constant, $\eta_x = 0$, η will trivially remain constant in the solution, $\eta_t = 0$. This property is easily inherited by *any* consistent discretization of (13), which makes (13) a suitable equation to use across the porosity jump where $[\eta] = 0$. We propose that across the porosity jump, the momentum equation be replaced by the entropy evolution equation (13). Away from the porosity jump, the flow reduces to two uncoupled single-phase Euler flows and generically is expected to develop shock waves. In these regions, we revert back to the conservative formulation. We therefore propose the following hybrid formulation:

(i) Away from the porosity jump solve

$$\begin{aligned} (\phi\rho)_t + (\phi\rho u)_x &= 0 \\ (\phi\rho u)_t + (\phi\rho u^2 + \phi p)_x &= p\phi_x \\ (\phi E)_t + (u(\phi E + \phi p))_x &= 0 \end{aligned} \tag{14}$$

(ii) Across the porosity jump solve

$$\begin{aligned} (\phi\rho)_t + (\phi\rho u)_x &= 0 \\ \eta_t + u\eta_x &= 0 \\ (\phi E)_t + (u(\phi E + \phi p))_x &= 0 \end{aligned} \tag{15}$$

We note that the energy flux may be written as $u(\phi E + \phi p) = \phi\rho uh$. It is straightforward to see that if the data correspond to a porosity wave, hence satisfy (9), all spatial derivatives in (15) vanish. Consequently, entropy, enthalpy and mass flow rate will remain constant in the analytic solution, as well as in any discrete

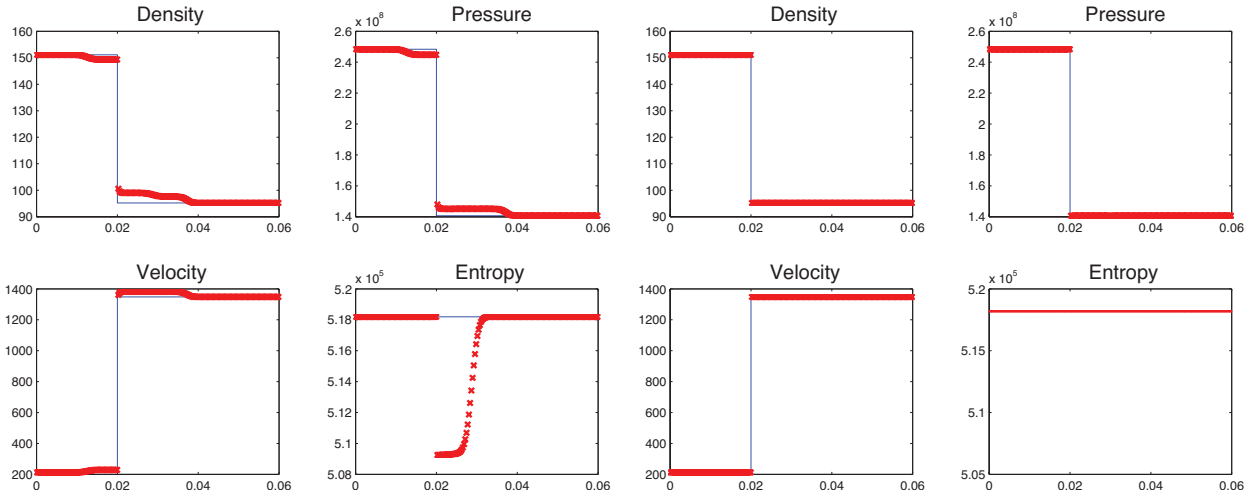

Figure 6: Computed and exact solutions corresponding to interface data (16): conservative (left) and hybrid (right) formulations.

approximation based on (15). Thus, data corresponding to compaction waves is recognized and respected by this formulation.

We also note that the conservative formulation is only used *away* from the porosity jump, hence the source term on its right hand side in fact vanishes and the system effectively reduces to two uncoupled standard Euler sub-systems.

The eigenvectors, eigenvalues and wave strengths for the conservative system are given by

$$R^C = \begin{pmatrix} 1 & 1 & 1 \\ u-c & u & u+c \\ h-uc & \frac{1}{2}u^2 & h+uc \end{pmatrix} \qquad \begin{aligned} \alpha_1^C &= \frac{\Delta\tilde{p} - \tilde{\rho}c\ \Delta u}{2c^2} \\ \alpha_2^C &= \frac{c^2\ \Delta\tilde{\rho} - \Delta\tilde{p}}{c^2} \\ \alpha_3^C &= \frac{\Delta\tilde{p} + \tilde{\rho}c\ \Delta u}{2c^2} \end{aligned} \qquad \Lambda = diag(u-c\ ,\ u\ ,\ u+c)$$

where we have used $\tilde{(\cdot)}$ to denote the respective quantities scaled by ϕ.

The eigenvectors of the nonconservative system (15) are derived in Appendix A. Decomposing $A\Delta W^{NC} = \sum_k \alpha_k\lambda_k r_k = \sum_k z_k r_k$ in terms of the Riemann invariants enables the scheme to recognize and respect porosity interface data. After some algebra we obtain the so-called f-wave strengths (see [10])

$$R^{NC} = \begin{pmatrix} 1 & 1 & 1 \\ 0 & -\frac{\gamma\eta}{\tilde{\rho}} & 0 \\ h-uc & \frac{1}{2}u^2 & h+uc \end{pmatrix} \qquad \begin{aligned} z_1 = \alpha_1\lambda_1 &= \frac{1}{2}\Delta\left(\tilde{\rho}u\right) + \frac{\tilde{p}\left(c+(\gamma-1)u\right)}{2(\gamma-1)\ \eta c^2}\Delta\eta - \frac{\tilde{\rho}}{2c}\Delta h \\ z_2 = \alpha_2\lambda_2 &= -\frac{\tilde{p}}{\eta c^2}\ u\Delta\eta \\ z_3 = \alpha_3\lambda_3 &= \frac{1}{2}\Delta\left(\tilde{\rho}u\right) - \frac{\tilde{p}\left(c-(\gamma-1)u\right)}{2(\gamma-1)\ \eta c^2}\Delta\eta + \frac{\tilde{\rho}}{2c}\Delta h \end{aligned}$$

4.2 Numerical Results

The next example corresponds to porosity interface data, extracted from the test in Figure 5.

$$\begin{array}{l} W_L = (1.5113 \times 10^2,\ 2.1231 \times 10^2,\ 2.4836 \times 10^8,\ 1.00) \\ W_R = (9.5199 \times 10^1,\ 1.3482 \times 10^3,\ 1.4067 \times 10^8,\ 0.25) \end{array} \tag{16}$$

Numerical and exact solution are shown in Figure 6, for the conservative (left) and hybrid (right) formulations. We note that the conservative formulation has difficulties keeping the entropy constant across the porosity jump, leading to erroneous waves structure. Using the entropy equation across the porosity jump and the conservative formulation everywhere else makes it possible to recognize and respect the interface data and produces a clean and error free solution.

We recompute the Riemann problem (12), this time with the hybrid formulation. Results are shown in Figure 5 (right) and are in excellent agreement with the exact solution, also shown. The hybrid formulation clearly recognizes and respects interface data, and yields the correct jump in the solution.

Figure 7 shows the computed solution by the hybrid scheme for two more Riemann problems. On the left, the solution for the initial data

$$\begin{array}{l} W_L = (1.0555, -1.0651, 1.5, 1.00) \\ W_R = (1.0000, -1.0000, 1.0, 1.25) \end{array} \tag{17}$$

corresponding to a left going rarefaction and a right going shock and on the right the solution for the initial data

$$\begin{array}{l} W_L = (0.6894, -1.6941, 1.5, 1.00) \\ W_R = (1.0000, -0.5000, 1.0, 1.25) \end{array} \tag{18}$$

producing a left and right moving rarefactions. In both examples, $\gamma = 1.4$, the CFL number is 0.8 and the grid has 400 points. Again, the jump in the solution across the interface is captured very well, and the computed solutions are in excellent agreement with the exact solutions, also shown.

5 Numerics - BN System

We now generalize the computational framework proposed in section 4 to the full Baer-Nunziato system (1). We propose the following strategy:

(i) Away from the compaction wave, solve for the conservative variables

$$W^C = (\phi_g \rho_g,\ \phi_g \rho_g u_g,\ \phi_g E_g,\ \phi_s \rho_s,\ \phi_s \rho_s u_s,\ \phi_s E_s,\ \phi_s)\ ; \tag{19}$$

(ii) Across the compaction wave, solve the nonconservative system in terms of the Riemann invariants

$$W^{RI} = (u_s,\ \eta_g,\ \eta_s,\ Q,\ P,\ H,\ \phi_s)\ . \tag{20}$$

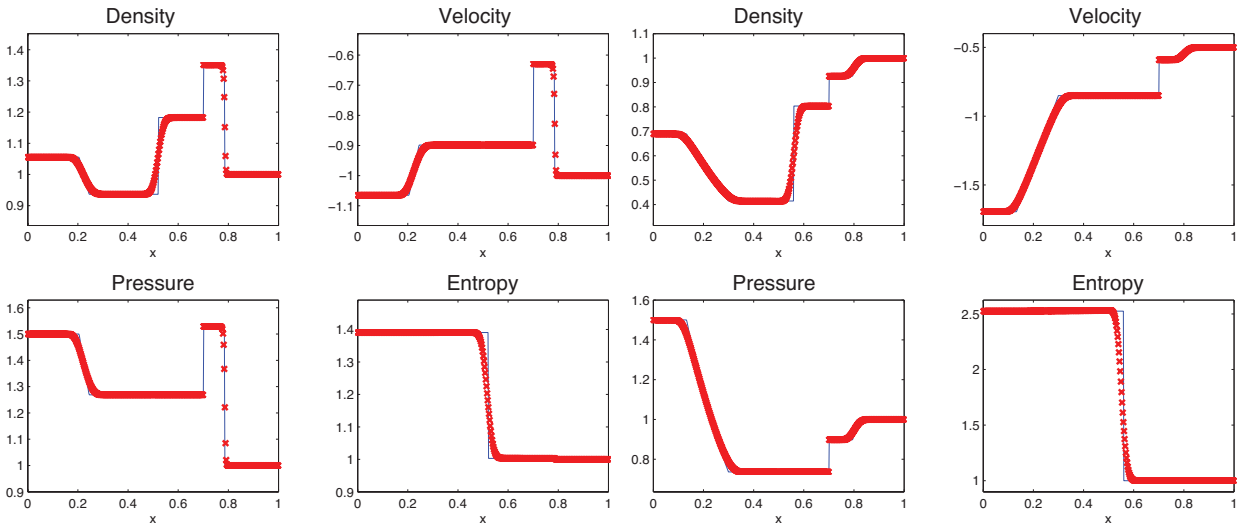

Figure 7: Computed and exact solutions corresponding to initial data (17) (left) and (18) (right).

The eigenvalues of the system are given in (4), the eigenvectors for the conservative formulation are given in (5). The corresponding wave strengths are

$$\alpha_1^C = \frac{\Delta\tilde{p}_g - \tilde{\rho}_g c_g \Delta u_g}{2c_g^2} - \frac{p_g(c_g + (\gamma_g - 1)v_g)}{2c_g^2(v_g - c_g)}\Delta\phi_s \qquad \alpha_2^C = \frac{-\Delta\tilde{p}_g + c_g^2\Delta\tilde{\rho}_g}{c_g^2} + \frac{(\gamma_g - 1)p_g}{c_g^2}\Delta\phi_s$$

$$\alpha_3^C = \frac{\Delta\tilde{p}_g + \tilde{\rho}_g c_g \Delta u_g}{2c_g^2} + \frac{p_g(c_g - (\gamma_g - 1)v_g)}{2c_g^2(v_g + c_g)}\Delta\phi_s$$

$$\alpha_4^C = \frac{\Delta\tilde{p}_s - \tilde{\rho}_s c_s \Delta u_s}{2c_s^2} - \frac{p_g}{2c_s^2}\Delta\phi_s \qquad \alpha_5^C = \frac{-\Delta\tilde{p}_s + c_s^2\Delta\tilde{\rho}_s}{c_s^2} - \frac{(\gamma_s - 1)p_s}{c_s^2}\Delta\phi_s$$

$$\alpha_6^C = \frac{\Delta\tilde{p}_s + \tilde{\rho}_s c_s \Delta u_s}{2c_s^2} - \frac{p_g}{2c_s^2}\Delta\phi_s$$

$$\alpha_7^C = \frac{1}{c_g^2 - v_g^2}\Delta\phi_s$$

where we have used $\tilde{(\cdot)}$ to denote the respective quantities scaled by the corresponding porosities $\phi_{g,s}$. The last eigenfield, corresponding to the compaction wave, does not play a significant role in the present context since it is proposed to use this formulation only away from the compaction wave front, where the porosity does not vary and α_7 vanishes. In that case, we also note that the rest of the wave strengths reduce to the standard expressions for the Euler system.

The eigenstructure in terms of the Riemann invariants W^{RI} is given by

$$R^{RI} = \begin{pmatrix} 0 & 0 & 0 & -1 & 0 & 0 & -1 \\ 0 & 1 & 0 & 0 & 0 & 0 & 0 \\ 0 & 0 & 0 & 0 & 1 & 0 & 0 \\ 1 & -v_g \dfrac{\tilde{p}_g}{\eta_g\, c_g^2} & 1 & \tilde{\rho}_g & 0 & 0 & \tilde{\rho}_g \\ v_g - c_g & -v_g^2 \dfrac{\tilde{p}_g}{\eta_g c_g^2} & v_g + c_g & 2\tilde{\rho}_g v_g + c_s \tilde{\rho}_s & 0 & 0 & 2\tilde{\rho}_g v_g - c_s \tilde{\rho}_s \\ -\dfrac{c_g}{\tilde{\rho}_g} & \dfrac{1}{\gamma_g - 1} \dfrac{\tilde{p}_g}{\eta_g\, \tilde{\rho}_g} & \dfrac{c_g}{\tilde{\rho}_g} & v_g & 0 & 0 & v_g \\ 0 & 0 & 0 & 0 & 0 & 1 & 0 \end{pmatrix}, \tag{21}$$

corresponding to the wave speed ordering $\Lambda = diag\,(u_g - c_g, u_g, u_g + c_g, u_s - c_s, u_s, u_s, u_s + c_s)$.

We note that the eigenfield corresponding to the double eigenvalue u_s is spanned by two linearly independent eigenvectors, one corresponding to the contact discontinuity carrying only changes in solid entropy η_s, and one corresponding to the compaction wave, carrying only changes in the porosity ϕ_s.

The wave strengths expressed in terms of W^{RI} are given by

$$\alpha_1 = -\frac{\tilde{\rho}_g\,(v_g - c_g)}{2c_g}\Delta u_s + \frac{\tilde{p}_g\,(c_g + (\gamma_g - 1)v_g)}{2(\gamma_g - 1)\eta_g c_g^2}\Delta\eta_g + \frac{1}{2}\Delta Q - \frac{\tilde{\rho}_g}{2c_g}\Delta H \quad \alpha_4 = -\frac{1}{2}\Delta u_s + \frac{M}{2\tilde{\rho}_s c_s}$$

$$\alpha_3 = \frac{\tilde{\rho}_g(v_g + c_g)}{2c_g}\Delta u_s - \frac{\tilde{p}_g\,(c_g - (\gamma_g - 1)v_g)}{2(\gamma_g - 1)\eta_g c_g^2}\Delta\eta_g + \frac{1}{2}\Delta Q + \frac{\tilde{\rho}_g}{2c_g}\Delta H \qquad \alpha_7 = -\frac{1}{2}\Delta u_s - \frac{M}{2\tilde{\rho}_s c_s}$$

$$\alpha_2 = \Delta\eta_g \quad \alpha_5 = \Delta\eta_s \quad \alpha_6 = \Delta\phi_s$$

where $M = \dfrac{\tilde{p}_g}{(\gamma_g - 1)\eta_g}\Delta\eta_g - v_g\Delta Q + \Delta P - \tilde{\rho}_g\Delta H$.

5.1 Numerical Examples

In all the following examples, initial data is given in terms of the primitive variables $W = (\rho_g, u_g, p_g, \rho_s, u_s, p_s, \phi_s)$.

Isolated Propagating Porosity Interface

The next example

$$\begin{aligned} W_L &= (1.0000, 2.0000, 0.5000, 2.0, 0.3,\ 5.000, 0.8) \\ W_R &= (0.2304, 2.4082, 0.0640, 3.0, 0.3, 13.0547, 0.3) \end{aligned} \tag{22}$$

corresponds to a *moving* compaction wave/solid contact, propagating with speed u_s . The CFL number is 0.8, the grid size is 400 points, and $\gamma_g = \gamma_s = 1.4$. It is not difficult to show that for an isolated moving compaction wave, the RI-formulation is in fact *exact*: it reduces to *linear advection* in the solid entropy and the porosity with advection speed u_s, and keeps the other variables constant. At the discrete level, this is reflected in the fact that for isolated interface data, all the wave strengths vanish except for α_5 and α_6, which reduce to $\alpha_5 = \Delta\eta_s$ and $\alpha_6 = \Delta\phi_s$. Figures 8 and 9 show the results by both the conservative and the hybrid formulation. The results clearly illustrate that the hybrid formulation recognizes and respects moving interface data. The Riemann invariants for the latter computation are shown in Figure 10 and confirm the ability of the formulation to treat correctly moving compaction waves.

We next consider Riemann problems corresponding to some degenerate wave configurations, here degeneracy in the sense that certain wave may be missing in the solution or that certain wave speeds may coincide. We examine the merit of the Riemann invariants based algorithm in these flow computations.

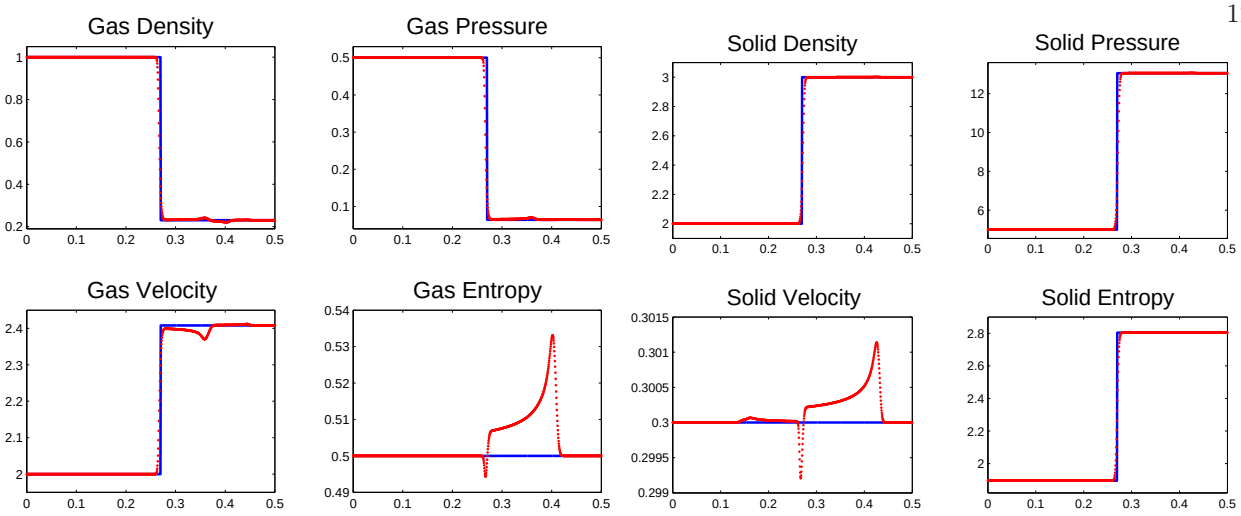

Figure 8: Computed and exact solutions for initial data (22) by the conservative formulation.

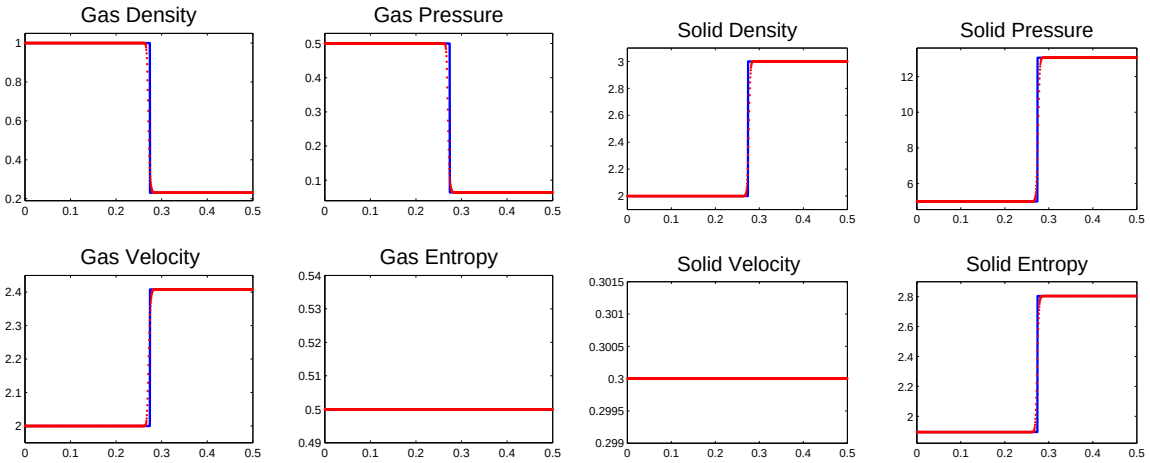

Figure 9: Computed and exact solutions for initial data (22) by the hybrid formulation.

Compaction Wave attached to a Gas Rarefaction

This degenerate case is a borderline case where the system loses strict hyperbolicity due to coinciding eigenvectors. The compaction wave is attached to the edge of the rarefaction fan in the gas, as illustrated in Figure 11. The initial data is given by

$$\begin{aligned} W_L &= (0.2800, -3.3761, 0.1051, 2.0, -1.0, 1.9990, 0.5) \\ W_R &= (0.4666, -2.6668, 0.2148, 0.5, -1.0, 8.3989, 0.1) \end{aligned} \tag{23}$$

following [5]. Results by the conservative formulation are shown in Figure 12, and exhibit errors near the compaction wave front. The solution shows noticeable improvement in resolving the compaction wave front in the hybrid formulation results, shown in Figure 13. Finally, as this example does not involve any shock waves, we have also computed solutions *entirely* by the nonconservative Riemann invariants formulation, whose eigenvectors are given by (21). The results are shown in Figure 14 and show further improvements over the hybrid formulation, indicating that some of the remaining errors in Figure 13 are in fact due to the conservative part of the hybridization.

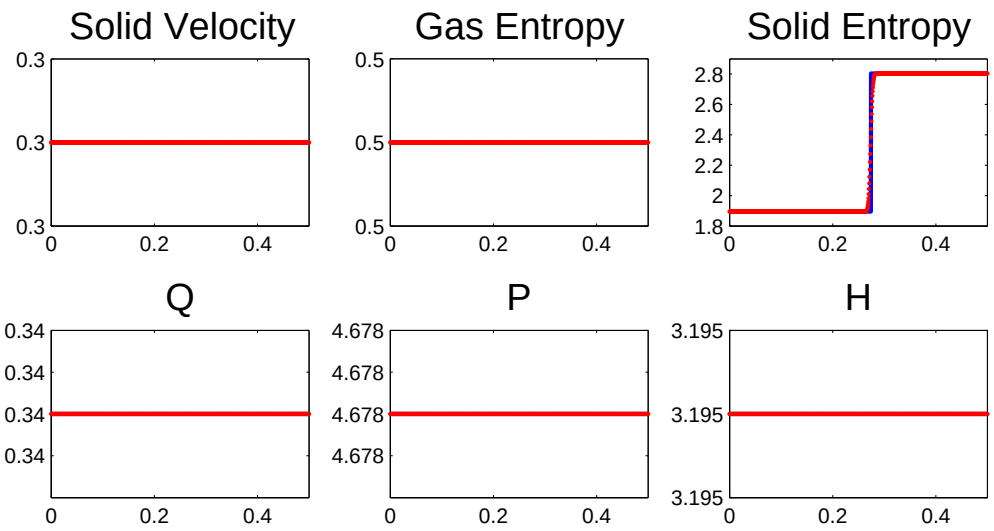

Figure 10: Computed and exact Riemann invariants for initial data (22) by hybrid formulation.

Stationary solid phase

The following initial data

$$\begin{aligned} W_L &= (5.92, -0.74, 6.680, 0.550,\ 0.00,\ 0.3504, 0.3) \\ W_R &= (2.02,\ \ 0.86, 1.870, 1.264, -0.115, 1.1234, 0.7) \end{aligned} \tag{24}$$

is taken from [8] and correspond to the Riemann solution in which the gas phase moves through a *stationary* solid phase, see schematic in Figure 15 (left).

Figures 16 and 17 show the computed and exact solutions by the conservative and hybrid formulation respectively. The challenge in this problem is to compute correctly the jump across the porosity interface. An additional and unrelated source of computational difficulty is the absence of certain waves from the solution, namely the acoustic waves in the solid phase. We note errors reminiscent of start-up errors, propagating at speeds corresponding to 'missing' waves, which can be observed in both sets of results. We can see that the hybrid strategy recognizes the Riemann invariant across the porosity interface, and produces a clean jump in the solution across the stationary interface at $x = 0.03$.

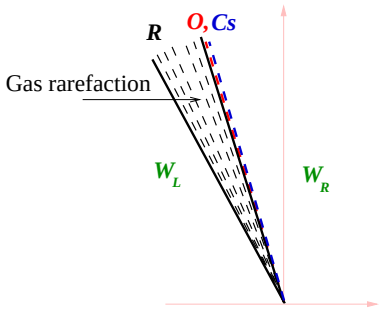

Figure 11: Schematic for a compaction wave right at the edge of a gas rarefaction fan.

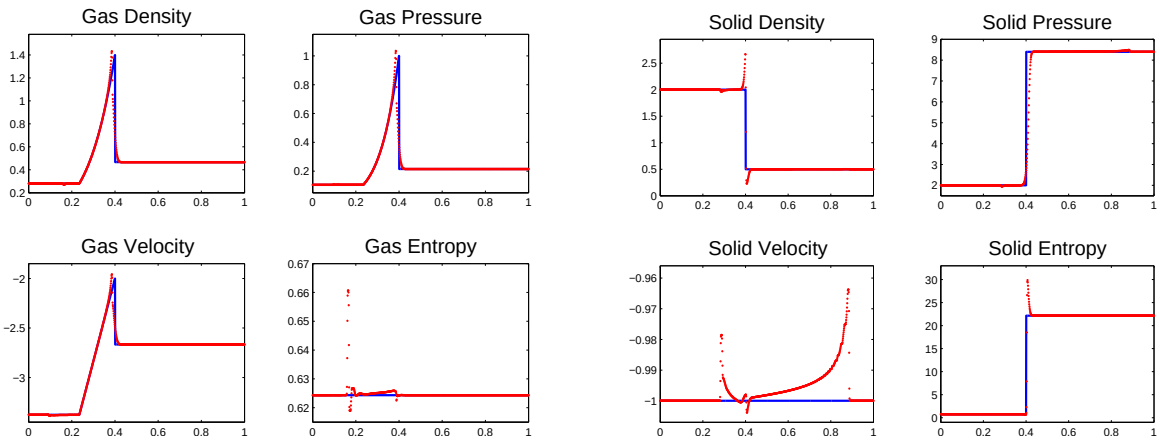

Figure 12: Numerical results for data (23) by conservative formulation.

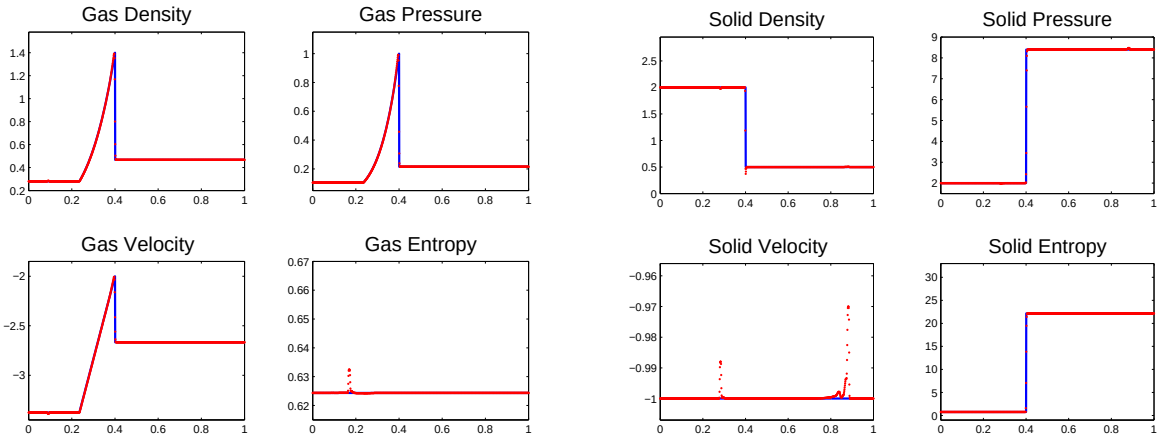

Figure 13: Numerical results for data (23) by hybrid formulation.

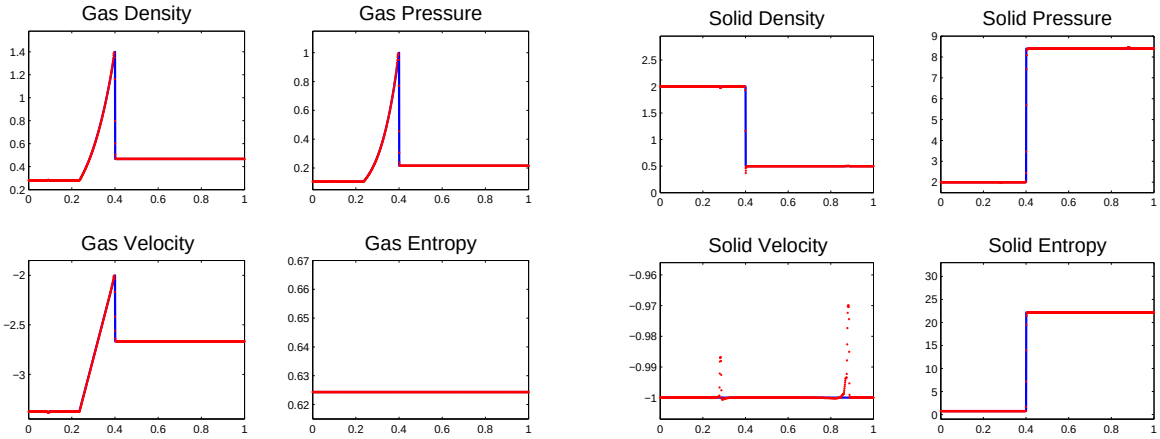

Figure 14: Numerical results for data (23) by the Riemann invariants formulation.

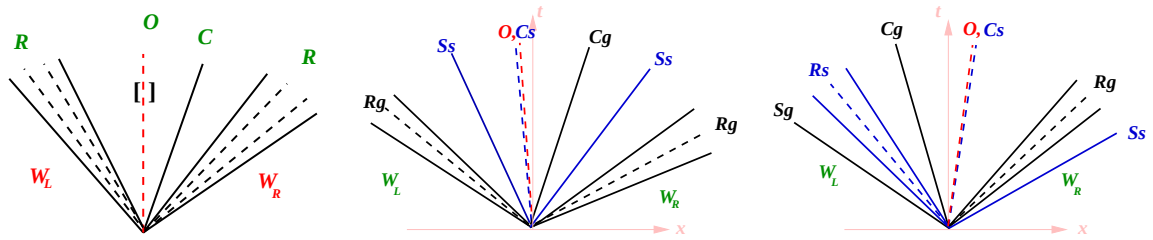

Figure 15: Schematic of solution corresponding to initial data (24) (left) , (25) (center) and (26) (right).

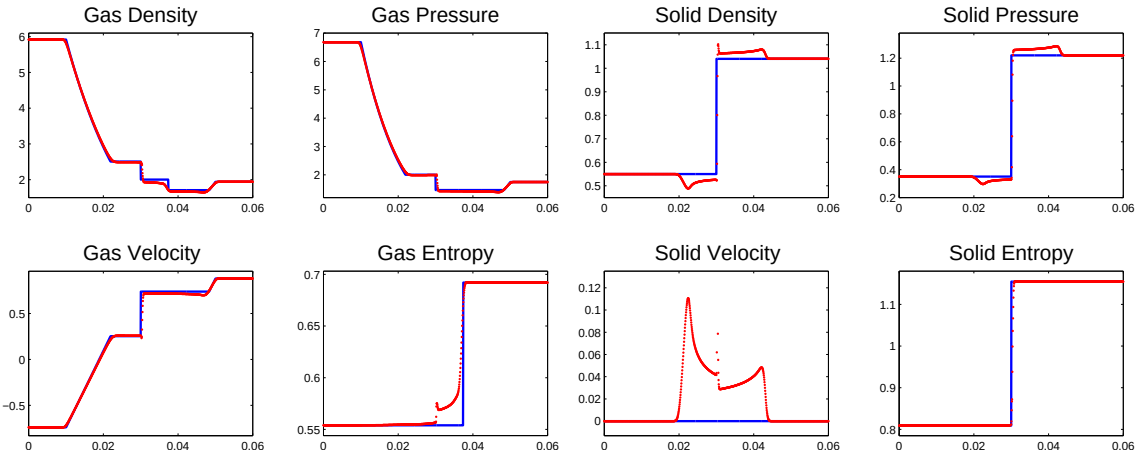

Figure 16: Computed and exact solutions corresponding to initial data (24) by the conservative formulation.

The following initial data

$$\begin{aligned} W_L &= (5.71, -0.75, 6.36, 0.553, -0.0553, 0.4527, 0.3) \\ W_R &= (1.94,\ 0.88, 1.75, 1.040,\ 0.00, 1.2200, 0.7) \end{aligned} \tag{25}$$

is taken from [8] and correspond to the Riemann solution schematic in Figure 15 (center). Figures 18 and 19 show the computed and exact solutions by the conservative formulation and the hybrid formulation respectively for data (25). In this case the interface is moving slightly to the left. The hybrid strategy produces clean solutions with the correct jumps at the interface.

Full Wave Configuration

The solution for the Riemann problem for the initial data (see [14])

$$\begin{aligned} W_L &= (0.2, 0, 0.3, 1, 0, 1, 0.8) \\ W_R &= (1, 0, 1, 1, 0, 1.01, 0.3) \end{aligned} \tag{26}$$

is depicted by the schematic in Figure 15 (right). Figures 20 and 21 show the exact and computed solutions for the conservative and hybrid formulations respectively.

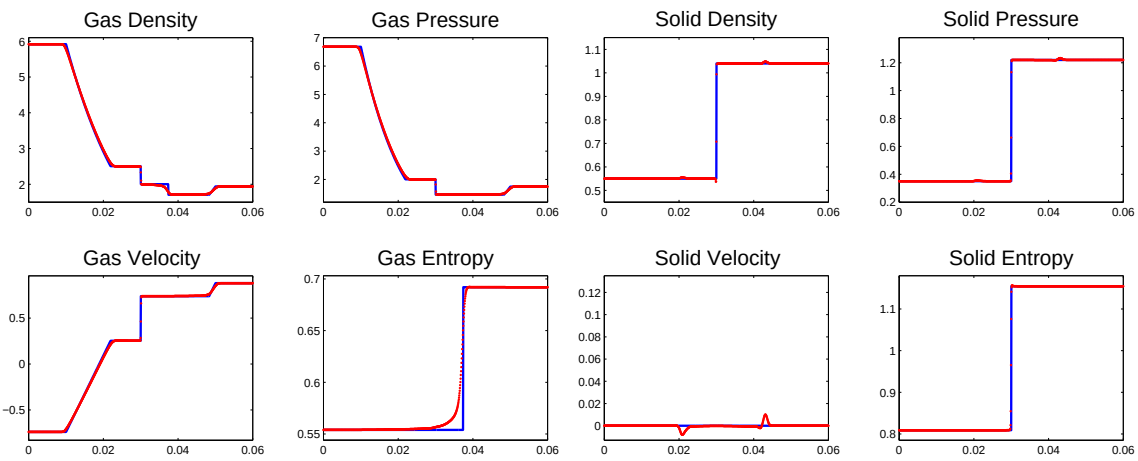

Figure 17: Computed and exact solutions corresponding to initial data (24) by the hybrid formulation.

Shock Refraction at a Porosity Interface

In this example, a shock wave in the gas phase propagates to the right and hits a porosity interface, see schematic in Figure 22. Initial data is given by

$$\begin{aligned} W_L &= (2.9330, 0.4136, 2.5000, 0.5476, 0.00, 0.3280, 0.3000) \\ W_M &= (2.5154, 0.2480, 2.0155, 0.5476, 0.00, 0.3280, 0.3000) \\ W_R &= (2.0462, 0.7114, 1.5096, 1.0400, 0.00, 1.2200, 0.7000) \end{aligned} \tag{27}$$

here W_M is the pre-shock state to the left of the porosity interface. Figures 23 and 24 show the computed solution by the conservative and hybrid formulations at a later time, after the shock has refracted at the porosity interface. Here, the conservative formulation is solved by the unsplit scheme with source upwinding proposed in [10], in which the source terms are projected onto the eigenvectors of the system. This solution is in visible error in computing the jump across the porosity interface, which results in inaccuracies in the other waves in the solution. The hybrid formulation produces a cleaner more accurate approximation.

Coinciding Shocks in Gas/Solid Phases

The following data

$$\begin{aligned} W_L &= (0.5806, 1.5833, 1.375, 0.2068, 1.4166, 0.0416, 0.1) \\ W_R &= (0.4890, -0.70138, 0.986, 2.2263, 0.9366, 6.0, 0.2) \end{aligned} \tag{28}$$

is taken from [5] and correspond to the eigenstructure on Figure 25. Here, both phases have left moving shock waves, which are moving at the same speed. The gas phase has a right moving shock which falls within a right moving rarefaction in the solid phase. Here $\gamma_g = \gamma_s = 1.4$. Results by the hybrid formulation are shown in Figure 26 and are in good agreement with the exact solution.

Shock Wave in gas near Compaction Wave

We expect the hybrid formulation not to perform well in wave configurations where the shock in the gas phase is moving with the same or close speed to the compaction wave. With this added degeneracy of an additional wave moving at the same speed as the compaction wave, the Riemann invariants are no longer constant across the combined wave front and the advantage of the formulation is lost. Furthermore, reverting to the nonconservative Riemann invariants solver may result in more noticeable conservation errors in the vicinity of the shock. The next data taken following [5] produces this type of solution (see schematic in Figure 27)

The initial data is

$$\begin{aligned} W_L &= (6.3311, -0.7890, 1.3244, 2.1917, -0.9950, 3.00, 0.5) \\ W_R &= (0.4141, -0.6741, 0.0291, 0.6333, -1.1421, 2.5011, 0.1) \end{aligned} \tag{29}$$

Here $\gamma_g = \gamma_s = 1.4$. Numerical results by the hybrid formulation are shown in Figure 28. Considering the fact that the hybrid formulation is ill-suited for this type of flow, the results are actually surprisingly good.

We conclude by making the following remarks:

Remark I:
In order to switch between the conservative and RI formulation, we need to track the compaction wave front. There are various ways to do that. In the computations presented in this paper, we have used gradient of the porosity ϕ_s to locate the interface. More specifically,

$$\left| \frac{\Delta \phi_s}{(\phi_s)_R - (\phi_s)_L} \right| < \epsilon,$$

for ϵ small, typically $\epsilon = 10^{-2} - 10^{-3}$.

Remark II:
Converting between the conservative and primitive variables in the case of multimaterial flow involves closed form explicit formulas (see [1]). In the present case, recovering the conservative set of variables from the Riemann invariants involves rootfinding of ρ_g in the equation

$$\frac{Q^2}{2\phi_g^2}\frac{1}{\rho_g^2} + \frac{\gamma_g}{\gamma_g - 1}\eta_g \rho_g^{\gamma_g - 1} - H = 0. \tag{30}$$

The equation may have more than one root, or no root at all. The latter may occur when intermediate states are generated when a large initial jump resolves itself into waves. By differentiating (30) with respect to ρ_g, it is possible to obtain a condition for the existence of the root, and identify data for which there is no root. In such cases, one may choose *not* to convert to the Riemann invariants and stick with the conservative formulation, thus avoiding altogether the need for rootfinding. Alternatively, since the initial data itself always permits going back and forth between conservative variables and Riemann invariants, one may repeat the calculation with a smaller time step Δt, typically half of the original Δt to allow the flow to resolve itself less abruptly.

References

[1] R.Abgrall and S. Karni, *Computations of Compressible Multifluids*, *Journal of Computational Physics*, **169**, 594-623 (2001).

[2] S. Karni, *Hybrid Multifluid Algorithms*, *SIAM J. Sci. Comput.*, **Vol. 17, No. 5**, 1019-1039 (1996).

[3] S. Karni, *Multicomponent flow calculations by a consistent primitive algorithm*, *J. Comput. Phys.*, **112**, 31-43 (1994).

[4] N. Andrianov and G. Warnecke, *On the solution to the Riemann problem for the compressible duct flow*, *SIAM Journal on Applied Mathematics*, **64** No. 3, 878-901 (2004).

[5] N. Andrianov and G. Warnecke, *The Riemann problem for the Baer-Nunziato two-phase flow model*, *Journal of Computational Physics*, **195**, 434-464 (2004).

[6] M. R. Baer and J. W. Nunziato, *A two-phase mixture theory for the deflagration-to-detonation transition (DDT) in reactive granular materials*, *International Journal of Multiphase Flow*, **12** No. 6, 861-889 (1986).

[7] P. Embid and M. R. Baer, *Mathematical analysis of a two-phase continuum mixture theory*, *Continuum Mechanics Thermodynamics*, **4**, 279-312 (1992).

[8] C. A. Lowe, *Two-phase shock-tube problems and numerical methods of solution*, *Journal of Computational Physics*, **204**, 598-632 (2005).

[9] G. Russo, *Central schemes for conservation laws with application to shallow water equations, in: S. Rionero, G. Romano (Eds.), Trends and Applications of Mathematics to Mechanics: STAMM 2002, Springer Verlag, Italia SRL, 2005*, 225-246.

[10] D. S. Bale, R. J. LeVeque, S. Mitran and J. A. Rossmanith, *A wave propagation method for conservation laws and balance laws with spatially varying flux functions*, *SIAM J. Sci. Comput.* **Vol. 24, No. 3**, 955-978 (2002).

[11] R. J. LeVeque , *Finite volume methods for hyperbolic problems*, *Cambridge University Press*, (2002).

[12] S. Noelle, Y. Xing, C. Shu, *High-order well-balanced finite volume WENO schemes for shallow water equation with moving water*, **226**, 29-58 (2007).

[13] P. L. Roe, *Approximate Riemann Solvers, Parameter Vectors, and Difference Schemes*, *Journal of Computational Physics*, **135**, 250-258 (1981).

[14] D. W. Schwendeman, C. W. Wahle and A. K. Kapila, , *The Riemann problem and a high-resolution Godunov method for a model of compressible two-phase flow*, *Journal of Computational Physics*, **212**, 490-526 (2006).

Appendix A: Eigenvectors for the Reduced System (15)

The eigenvectors of different formulations of the hyperbolic system (6) are related through the Jacobian matrix of the nonlinear transformation between the respective sets of the dependent variables. Here, we obtain the eigenvectors of (15) by an equivalent but more direct calculation.

We first note that across the k^{th} simple wave, $\delta W \sim r_k$, implying, for example that across a 1-wave, a small change in the density, $\delta\tilde{\rho}$, is accompanied by a $(u-c)\delta\tilde{\rho}$ change in the momentum, $\tilde{\rho}u$, and a $(h-uc)\delta\tilde{\rho}$ change in the energy $\tilde{E}$. Alternatively, across a 1-wave, using the eigenvectors for the primitive formulation (7), a small change in the density $\delta\rho$ is accompanied by a small change in velocity $\delta u = -(c/\rho)\delta\rho$ and a small change in pressure $\delta p = c^2\delta\rho$, but no change in porosity $\delta\phi = 0$. A similar interpretation applies to the other waves.

To obtain r_1^{NC} for the nonconservative set of variables $W^{NC} = (\tilde{\rho}, \eta, \tilde{E})$, we observe that

$$\delta\tilde{\rho} = \delta\phi\rho = \phi\delta\rho + \rho\delta\phi = \phi\delta\rho$$

and using logarithmic differentiation of $\eta = p\rho^{-\gamma}$ we get

$$\frac{\delta\eta}{\eta} = \frac{\delta p}{p} - \gamma\frac{\delta\rho}{\rho} = \frac{c^2\delta\rho}{p} - \gamma\frac{\delta\rho}{\rho} \equiv 0$$

implying that a 1-wave does not carry any changes in entropy. The first eigenvector for the nonconservative formulation (15) is therefore $r_1^{NC} = (1, 0, h-uc)$. The calculation for the 3-wave is practically identical. For the 2-wave, a similar calculation gives

$$\frac{\delta\eta}{\eta} = \frac{\delta p}{p} - \gamma\frac{\delta\rho}{\rho} = -\gamma\frac{\delta\rho}{\rho} = -\gamma\frac{\delta\tilde{\rho}}{\tilde{\rho}}$$

implying that across a 2-wave

$$\delta\eta = -\frac{\gamma\eta}{\tilde{\rho}}\delta\tilde{\rho}.$$

Combining results together, we obtain

$$R^C = \begin{pmatrix} 1 & 1 & 1 \\ u-c & u & u+c \\ h-uc & \frac{1}{2}u^2 & h+uc \end{pmatrix} \qquad R^{NC} = \begin{pmatrix} 1 & 1 & 1 \\ 0 & -\frac{\gamma\eta}{\tilde{\rho}} & 0 \\ h-uc & \frac{1}{2}u^2 & h+uc \end{pmatrix}$$

The wave strengths α_k are obtained as follows. Away from the porosity jump, the wave strengths for the conservative formulation are given by the familiar expressions

$$\alpha_1^C = \frac{\delta\tilde{p} - \tilde{\rho}c\ \delta u}{2c^2}, \quad \alpha_2^C = \frac{c^2\delta\tilde{\rho} - \delta\tilde{p}}{c^2}, \quad \alpha_3^C = \frac{\delta\tilde{p} + \tilde{\rho}c\delta u}{2c^2}$$

Near the interface, we express the wave strengths in terms of the Riemann invariants $\tilde{\rho}u$, η and h. This guarantees the preservation of interface data.

$$A^{NC}\delta W^{NC} = \begin{pmatrix} \delta(\tilde{\rho}u) \\ u\delta\eta \\ \delta(\tilde{\rho}uh) \end{pmatrix} = \begin{pmatrix} \delta(\tilde{\rho}u) \\ u\delta\eta \\ \tilde{\rho}u\delta h\ +\ h\delta\tilde{\rho}u \end{pmatrix} = \sum \alpha_k\lambda_k r_k^{NC}$$

A simple calculation gives

$$\begin{aligned} z_1 = \alpha_1\lambda_1 &= \frac{1}{2}\delta(\tilde{\rho}u) + \frac{\tilde{p}\,(c + (\gamma-1)u)}{2(\gamma-1)\ \eta c^2}\delta\eta - \frac{\tilde{\rho}}{2c}\delta h \\ z_2 = \alpha_2\lambda_2 &= -\frac{\tilde{p}}{\eta c^2}\ u\delta\eta \\ z_3 = \alpha_3\lambda_3 &= \frac{1}{2}\delta(\tilde{\rho}u) - \frac{\tilde{p}\,(c - (\gamma-1)u)}{2(\gamma-1)\ \eta c^2}\delta\eta + \frac{\tilde{\rho}}{2c}\delta h, \end{aligned}$$

as desired.

The eigenvectors for both the conservative and non-conservative formulation for the full system (19) and (20) are obtain in an analogous way, and are given in section 5.

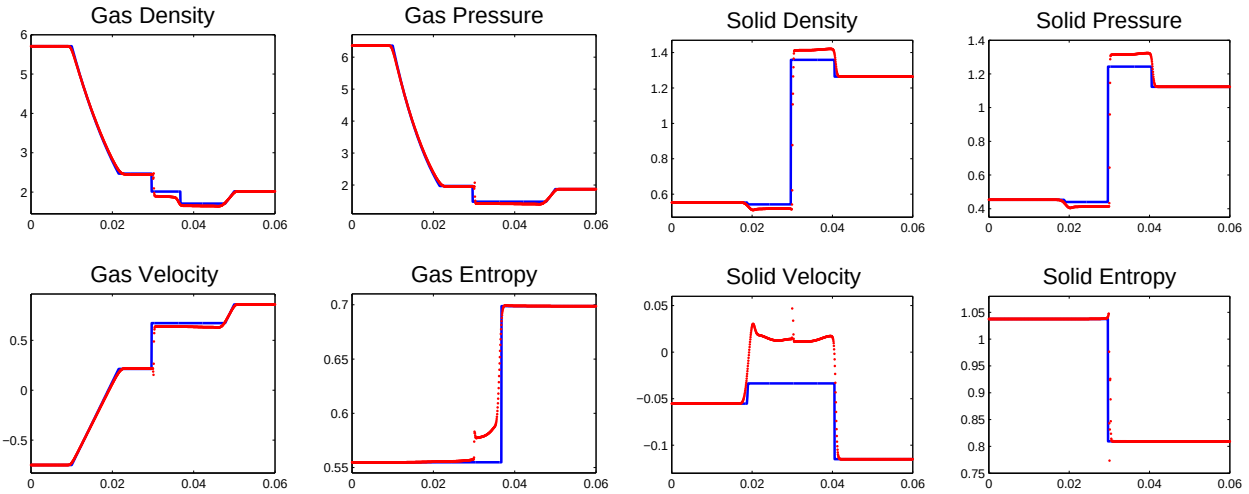

Figure 18: Computed and exact solutions corresponding to initial data (25) by the conservative formulation.

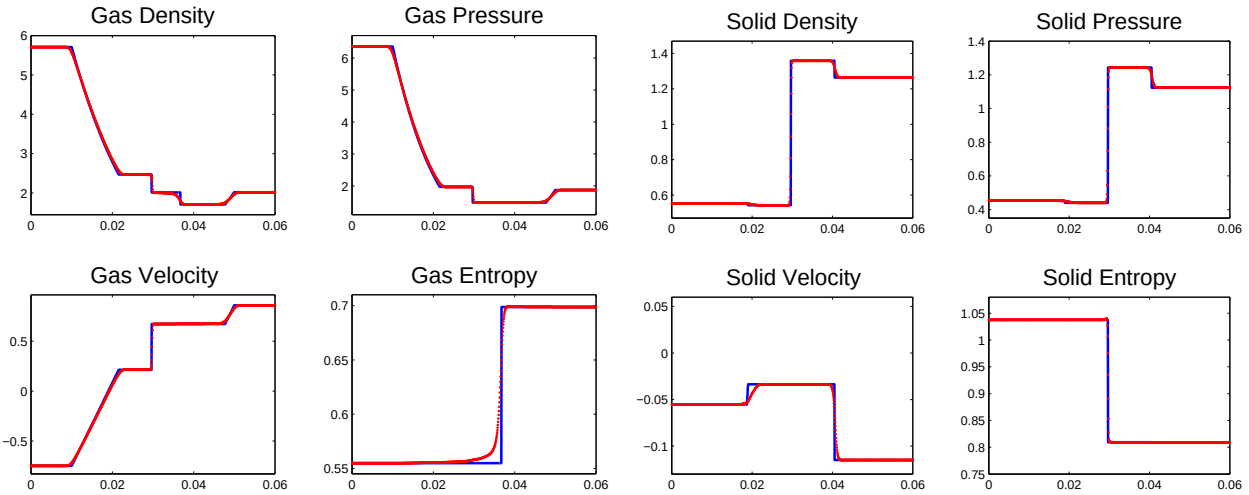

Figure 19: Computed and exact solutions corresponding to initial data (25) by the hybrid formulation.

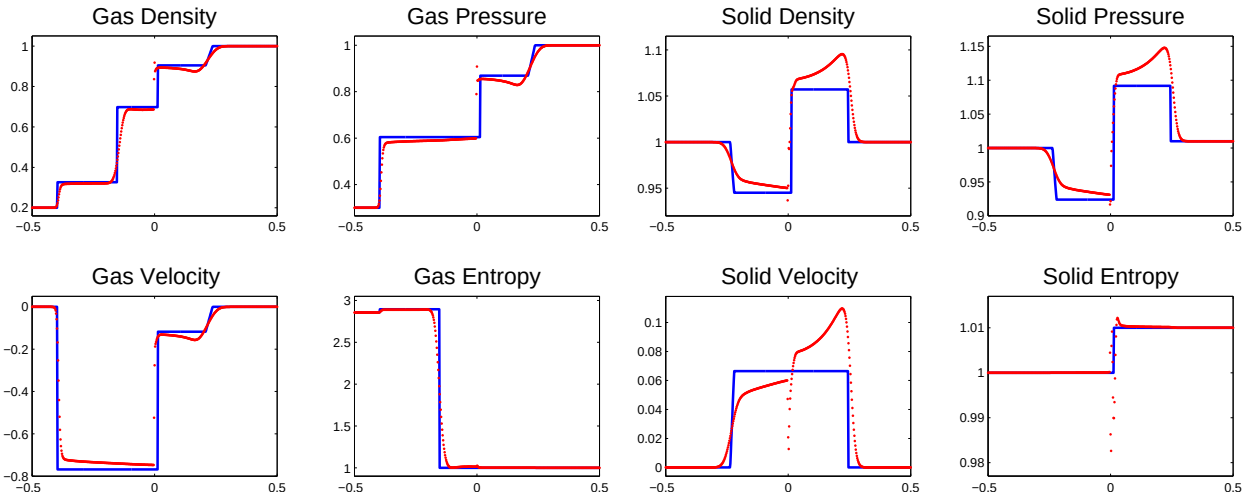

Figure 20: Computed and exact solutions corresponding to initial data (26) by the conservative formulation.

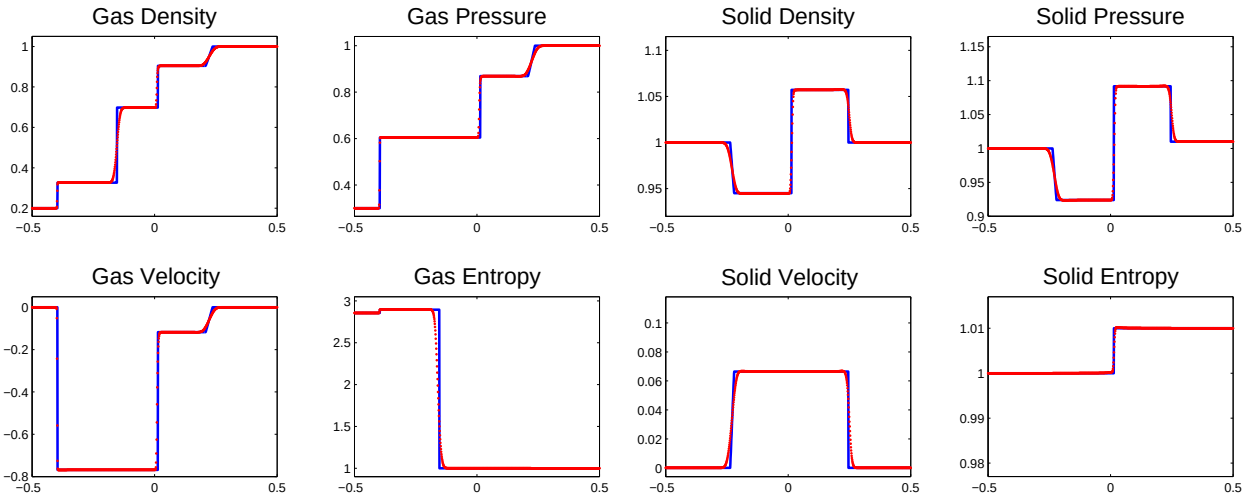

Figure 21: Computed and exact solutions corresponding to initial data (26) by the hybrid formulation.

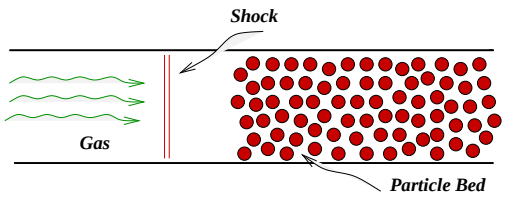

Figure 22: A shock hitting a porosity jump.

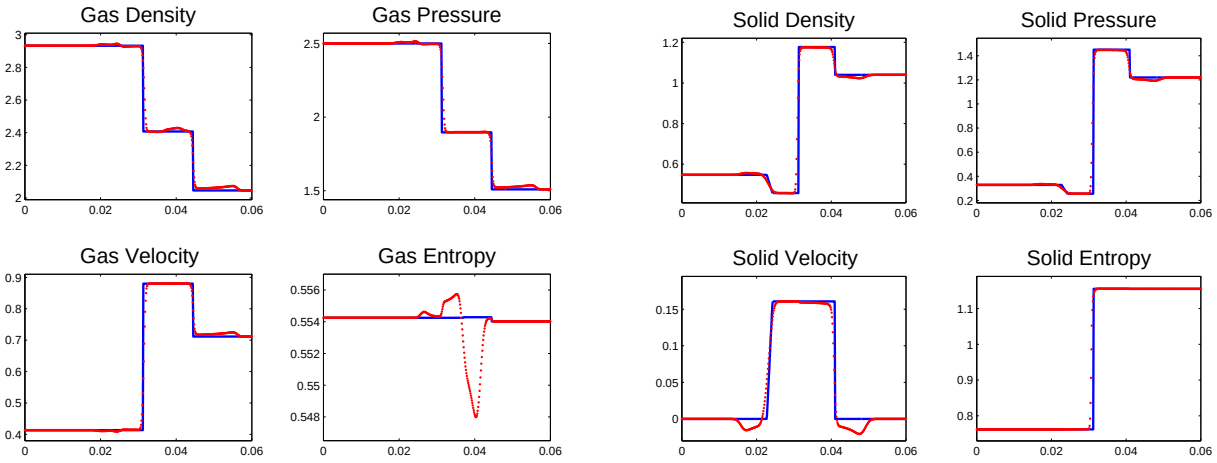

Figure 23: A shock refracting at a porosity interface . Conservative method.

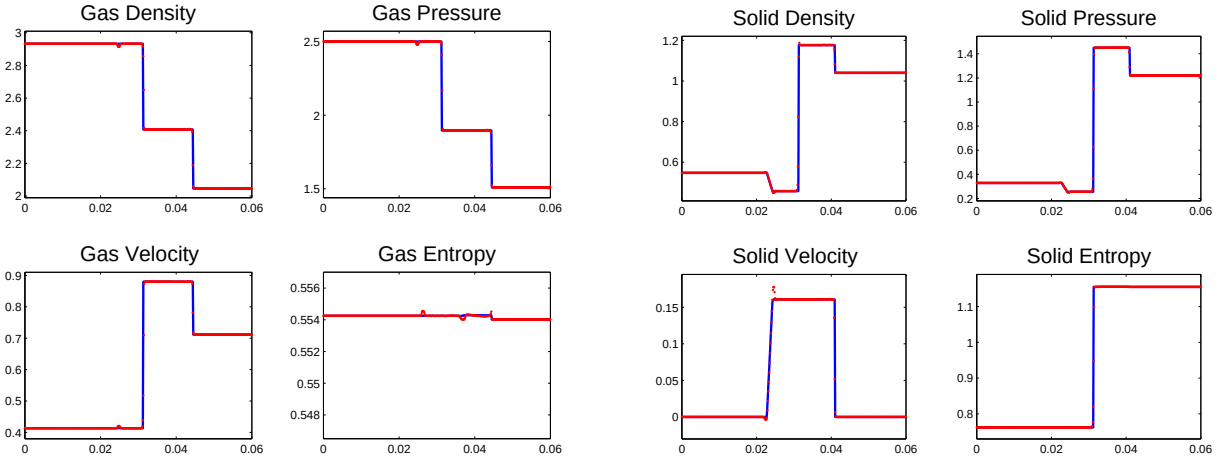

Figure 24: A shock refracting at a porosity interface. Hybrid method.

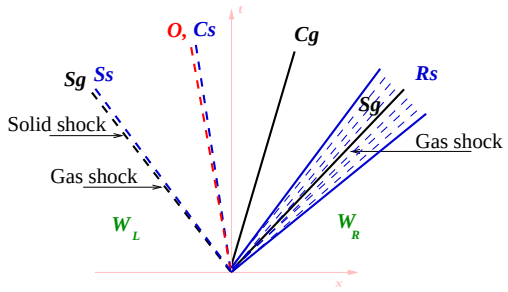

Figure 25: Schematic of solution corresponding to initial data (28), coinciding shock and rarefactions.

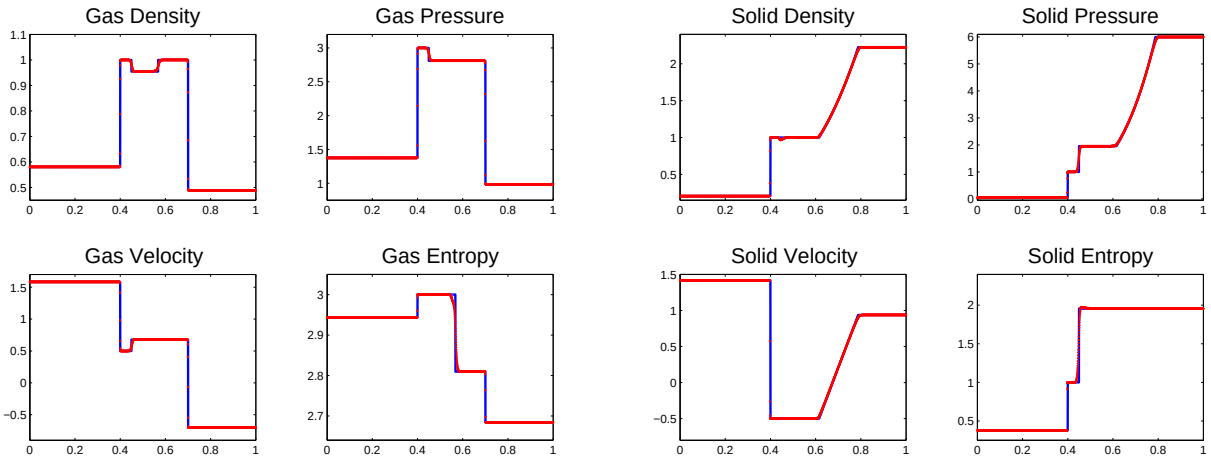

Figure 26: Computed ans exact solution corresponding to data (28). Hybrid formulation.

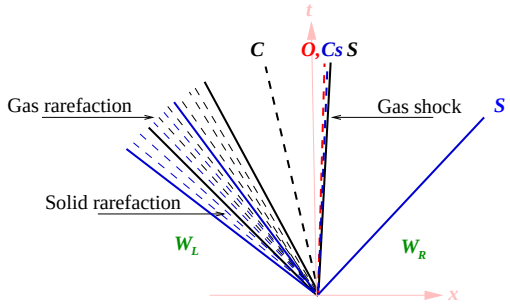

Figure 27: Schematic for data in (29), shock wave in gas near a compaction wave.

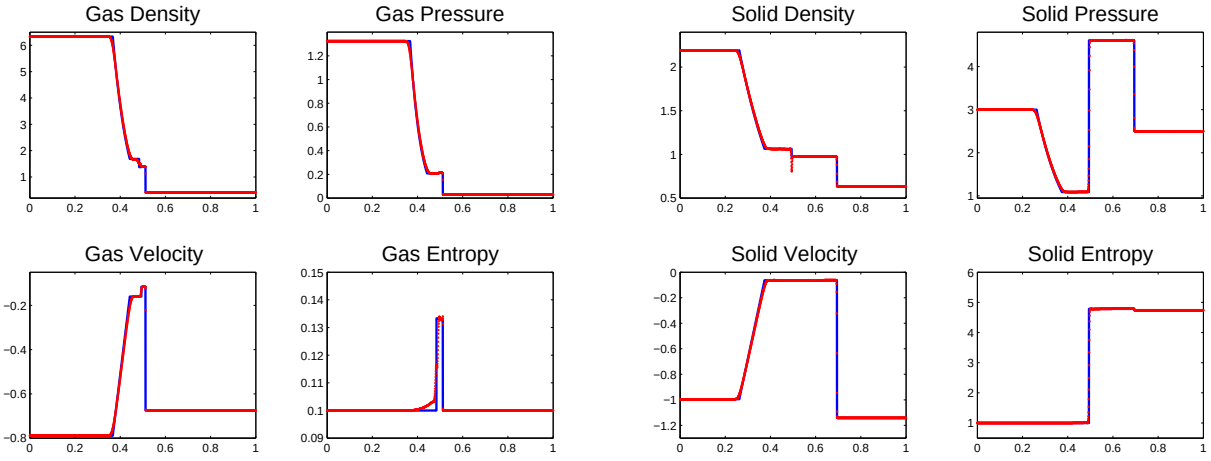

Figure 28: A shock wave in gas near a compaction wave. Numerical results for data (29) by hybrid method.